Scaling Miscible Fluid Displacements in Porous Media

ARTICLE *in* ENERGY & FUELS · JUNE 1998

Impact Factor: 2.79 · DOI: 10.1021/ef980020a

3 AUTHORS, INCLUDING:

A. Elkamel
University of Waterloo
306 PUBLICATIONS **2,148** CITATIONS

Scaling Miscible Fluid Displacements in Porous Media

Ridha Gharbi,*,† Ekwere Peters,‡ and Ali Elkamel§

Departments of Petroleum Engineering and Chemical Engineering, Kuwait University, P.O. Box 5969, Safat 13060, Kuwait, and Center for Petroleum & Geosystems Engineering, The University of Texas at Austin, Austin, Texas 78712

Received January 29, 1998. Revised Manuscript Received April 30, 1998

The importance of miscible displacements in the petroleum industry makes their understanding and quantitative prediction critical in decisions on the applicability of certain recovery techniques. In this study, scaling miscible displacements in porous media was investigated using a general procedure of inspectional analyis. The procedure was used to derive the minimum number of dimensionless scaling groups which govern miscible displacements. It was found that scaling miscible displacements in a two-dimensional, homogeneous, anisotropic vertical cross-section requires the matching of nine dimensionless scaling groups. A numerical sensitivity study of the equations was performed to investigate the effects of some of the scaling groups on the performance of miscible displacements. Through this sensitivity study, it was found that one of the groups is insensitive to the results over all practical values. Hence, the problem can be scaled by only eight dimensionless scaling groups. The prediction of the recovery efficiency for miscible EOR processes can be achieved solely by analyzing these scaling groups. Preliminary results indicate that when the groups are used as inputs to an artificial neural network, the efficiency of the displacement can be accurately predicted.

Introduction

It is generally recognized that at the end of a conventional secondary recovery, almost 65−70% of residual oil will remain in the reservoir.[1−3] Enhanced oil recovery (EOR) is used to recover as much as possible of this residual oil. The enhanced oil recovery methods can be divided into three major groups: thermal, chemical, and solvent methods. For each of these methods there is one major problem that must be overcome to recover a significant part of the remaining oil. This problem is to achieve microscopic recovery efficiency to displace the oil from the rock matrix and cause it to flow through the formation along a specific pathway.

Thermal recovery methods add heat to the reservoir (by the use of steam or in situ combustion) to reduce the viscosity of the oil. Solvent recovery methods are based on injecting fluids that mix with the oil under reservoir conditions to reduce viscosity. Examples of these fluids include carbon dioxide, light hydrocarbons, and nitrogen. Chemical EOR methods are based on the injection of chemicals that reduce interfacial tensions hence favoring oil production.

In order to check the effectiveness of various EOR processes before they are tried in the field, a comprehensive understanding and characterization of the process must be available. This understanding comes from analyzing the parameters affecting the EOR process behavior. In our earlier studies,[4−6] we have investigated immiscible EOR processes. The important scaling groups affecting these processes have been determined and used as input parameters to artificial neural network (ANN) prediction models. These ANN models serve to perform a quick preliminary study for selecting a given immiscible EOR process and can also be integrated within general software packages for scheduling and planning oil production operations. In addition, the neural network models have been shown to be able to optimize a given EOR process by invoking their inverse property.[7] Optimizing an EOR process is the determination of the manipulated reservoir conditions that will lead to the best recovery. The utility of ANNs as quick predictive tools stems from the fact that a planning software for oil production needs to be furnished with recovery predictions continuously before being able to determine the optimal plan of operation. Convergence to an optimal solution might be obtained only after hundreds of iterations. For each iteration, the recovery is calculated as a function of the conditions

† Department of Petroleum Engineering, Kuwait University.
‡ Department of Chemical Engineering, Kuwait University.
§ The University of Texas at Austin.

(1) Shah, D. O. *Surface Phenomena in Enhanced Oil Recovery*; Plenum Press: New York, 1981.
(2) Lake, L. W. *Enhanced Oil Recovery*; Prentice-Hall: Englewood Cliffs, NJ, 1989.
(3) Amundson, N. R. Frontiers in Chemical Engineering: Research Needs and Opportunities; National Academy Press: Washington, DC, 1988.
(4) Peters, E. J.; Afzal, N.; Gharbi, R. On Scaling Immiscible Displacements in Permeable Media. *J. Pet. Sci. Eng.* **1993**, *9* (3), 183−205.
(5) Gharbi, R.; Karkoub, M.; Elkamel, A. An Artificial Neural Network for the Prediction of Immiscible Flood Performance. *Energy Fuels* **1995**, *9*, 894.
(6) Elkamel, A.; Karkoub, M.; Gharbi, R. A Neural Network Prediction Model of Fluid Displacements in Porous Media. *Comput. Chem. Eng.* **1996**, *20*, 5515.
(7) Elkamel, A. An Artificial Neural Network for Predicting and Optimizing Immiscible Flood Performance in Heterogeneous Reservoirs. Presented at the Simulation Multiconference, Atlanta, GA, 1997.

S0887-0624(98)00020-6 CCC: $15.00
Published on Web 06/16/1998

and parameters of the reservoir. If only a reservoir simulator is available to perform these predictions, the computational expenses become prohibitively large.

The purpose of the present paper is to take the initial steps in preparing prediction tools (i.e. ANNs) for miscible EOR processes. To do so, the dimensionless scaling groups that characterize the flow must first be determined. In general, two methods may be used to derive the dimensionless scaling groups: inspectional analysis,[8,9] which is based on the differential equations that govern the displacement, and dimensional analysis,[10−12] which is based on a knowledge of the pertinent variables affecting the displacement.

Inspectional analysis is performed by rendering the differential equations of the displacement together with the initial and boundary conditions into dimensionless forms. This can be done by the introduction of appropriate normalizing variables. The result is the appearance of dimensionless dependent variables, dimensionless independent variables, and dimensionless similarity or scaling groups. On the other hand, dimensionless analysis does not require that the process being modeled be expressed by equations. Instead, only a knowledge of the pertinent variables is required.[10−12] The dimensionless groups are derived by requiring that the power products of the variables be dimensionless. This requirement results in a homogeneous system of linear algebraic equations, the solution of which yields a complete set of independent, though not unique, dimensionless groups. The number of dimensionless groups that can be formed from a set of variables is given by Buckingham's π theorem.

Both methods of deriving the scaling laws have their advantages and limitations.[13] Inspectional analysis usually gives rise to scaling groups whose physical significance is readily apparent, whereas dimensional analysis may give rise to groups whose physical significance may be quite obscure. For example, based on the locations of the scaling groups in the dimensionless differential equations, it is easy to identify that a certain similarity group is the ratio of the capillary to the viscous forces or the gravitational to the viscous forces. On the other hand, inspectional analysis, unlike dimensional analysis, does require a mathematical equation for the process under study. If such an equation is unavailable, inspectional analysis cannot begin, whereas dimensional analysis can still provide some guidance in setting up experiments to initiate the study. In any case, even when a differential equation is available, it is usually only the aspect of a well-understood phenomenon that is modeled. As a result, the scaling groups derived from inspectional analysis may be incomplete. Therefore, dimensional analysis is much more general than inspectional analysis, and in this generality lies its strength and its weakness. When very little theory is available, dimensional analysis can be relied upon to provide initial guidance in setting up experiments. However, it is so general that the inclusion of superfluous variables in the list of pertinent variables will give rise to superfluous but no less legitimate scaling groups.

Extensive literature is available on the subject of scaling that is applicable to multiphase flow in porous media.[13−26] The use of dimensionless groups in the investigation of immiscible displacements of oil by water was initiated by Leverett et al.[19] and then extended by Engleberts and Klinkenberg.[26] Croes and Schwarz[16] presented a detailed study on the influence of the oil/water viscosity ratio on immiscible displacements. They presented a diagram from which the cumulative oil recovery can be read for water−oil viscosity ratios ranging from 1 to 500. However, the diagram is applicable only to homogeneous reservoirs produced by linear displacement of oil by water. Offeringa and Van Der Poel[27] presented scaled results of oil recovery by miscible displacement.

The first successful attempt to use inspectional analysis in the immiscible displacement of oil by cold water was given by Rapoport.[22] This work was later extended by Geertsma et al.[17] to include hot water displacement and solvent flooding. The authors used a procedure that combined inspectional analysis with dimensional analysis to derive the dimensionless similarity groups for these types of production mechanisms. In their scaling study, Craig et al.[28] included anisotropy to investigate the effects of gravity segregation in miscible and immiscible displacements in five-spot models. They presented a correlation between the ratio of vertical to horizontal pressure gradient and the oil recovery at

(8) Ruark, A. E. Inspectional Analysis: A Method Which Supplements Dimensional Analysis. *J. Elisha Mitchell Sci. Soc.* **1935**, *51*, 127−132.

(9) Birkhoff, G. *Hydrodynamics: A Study in Logic, Fact, and Similitude*; Princeton University Press: Princeton, NJ, 1950.

(10) Buckingham, E. On Physically Similar Systems; Illustrations of the Use of Dimensional Equations. *Phys. Rev.* **1914**, *4*, 345.

(11) Focken, C. M. *Dimensional Methods and Their Applications*; Arnold & Co.: London, 1953.

(12) Langhaar, H. L. *Dimensional Analysis and Theory of Models*; John Wiley & Sons: New York, 1951.

(13) Bear, J. *Dynamics of Fluids in Porous Media*; Elsevier Publishing Co., Inc.: New York, 1972; pp 665−727.

(14) Carpenter, C. W., Jr.; Bail, P. T.; Bobek, J. E. A Verification of Waterflood Scaling in Heterogeneous Communicating Flow Models. *Soc. Pet. Eng. J.* **1962**, *2*, 9−12.

(15) Collins, R. E. *Flow of Fluids Through Porous Materials*; The Petroleum Publishing Company: Tulsa, OK, 1976; pp 217−241.

(16) Croes, G. A.; Schwarz, N. Dimensionally Scaled Experiments and the Theories on the Water-Drive Process. *Trans. AIME* **1955**, *204*, 35−42.

(17) Geertsma, J.; Croes, G. A.; Schwarz, N. Theory of Dimensionally Scaled Models of Petroleum Reservoirs. *Trans., AIME* **1956**, *207*, 118−127.

(18) Greenkorn, R. A. Flow Models and Scaling Laws?Flow Through Porous Media. *Ind. Eng. Chem.* **1964**, *56*, 27−32.

(19) Leverett, M. C.; Lewis, W. B.; True, M. E. Dimensional-Model Studies of Oil-Field Behavior. *Trans. AIME* **1942**, *146*, 175−193.

(20) Loomis, A. G.; Crowell, D. C. Theory and Application of Dimensional and Inspectional Analysis to Study Displacements in Petroleum Reservoirs. U. S. Bureau of Mines, Report of Investigation 6546, 1964.

(21) Nielsen, R. L.; Tek, M. R. Evaluation of Scale-Up Laws for Two-Phase Flow Through Porous Media. *Soc. Pet. Eng. J.* 1963, June, 164−176.

(22) Rapoport, L. A. Scaling Laws for Use in Design and Operation of Water−Oil Flow Model. *Trans. AIME* **1955**, *204*, 143−150.

(23) Rapoport, L. A.; Leas, W. J. Properties of Linear Waterfloods. *Trans. AIME* **1953**, *198*, 139−148.

(24) Wygal, R. J. Construction of Models that Simulate Oil Reservoirs. *Soc. Pet. Eng. J.* **1963**, *3*, 281−286.

(25) Shook, M.; Li, D.; Lake, W. L. Scaling Immiscible Flow Through Permeable Media by Inspectional Analysis. *In Situ* **1992**, *16* (3), 311−349.

(26) Engelberts, W. F.; Klinkenberg, L. J. Laboratory Experiments on the Displacement of Oil by Water from Packs of Granular Materials. Proceedings of Third World Petroleum Congress, Sec. II, The Hague, 1951, pp 544−554.

(27) Offeringa, J.; van der Poel, C. Displacement of Oil from Porous Media by Miscible Liquids. *Trans. AIME* **1954**, *201*, 310−315.

(28) Craig, F. F.; Sanderlin, J. L.; Moore, D. W.; Geffen, T. M. A Laboratory Study of Gravity Segregation in Frontal Drives. *Trans. AIME* **1957**, *210*, 275−282.

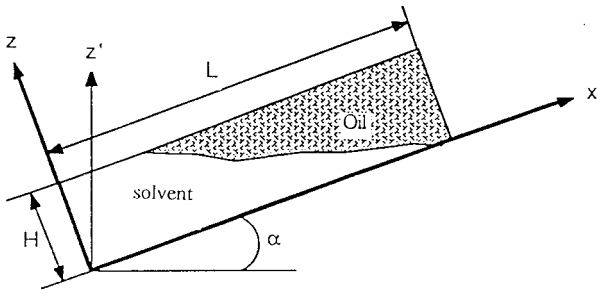

Figure 1. Oil displacement in a two-dimensional porous medium.

breakthrough for various mobility ratios. In addition, a correlation between the experimental oil recovery and a dimensionless gravity number was presented for five-spot miscible displacements. In 1960, Perkins and Collins[29] presented scaling criteria which allow the relative permeability and the capillary pressure curves of the model to be different from those of the prototype. Van Daalen and Van Domslaar[30] used inspectional analysis to study scaling of models that have different geometries from that of the prototype. They found that if no cross-flow occurs, then the aspect ratio is not important in scaling immiscible displacements. However, if cross-flow occurs, then the aspect ratio becomes important in scaling immiscible displacements.

Despite all these published works, there are still inconsistencies about the number of dimensionless scaling groups required to describe a specific miscible displacement process and in the definition of these scaling groups. In this paper, dimensionless scaling groups for miscible displacements in porous media are obtained using a generalized procedure.[25] These groups were validated through sensitivity analysis studies. For different parameter sets leading to the same numerical value of a certain group, the effects on the oil recovery were observed to be identical. The variations of oil recovery in terms of selected groups will be given in detail. The variations study was specifically done on these groups because of the lack of information about their effects in the current literature.

Derivation of the Dimensionless Scaling Groups

Consider a miscible displacement of incompressible fluids in a two-dimensional porous medium. The medium is assumed to be homogeneous and anisotropic (diagonal permeability tensor, $k_x \neq k_z$) with a dip angle α measured from the horizontal. The x-axis is the principle flow direction, while the z-axis is the direction perpendicular to the flow (assuming $x \gg y$). Figure 1 shows the geometrical setting. The pore space of the medium is initially filled with a displaced fluid ($C = 0$) and flooded at the side $x = 0$ with a displacing fluid ($C = 1$). Furthermore, for the sake of generality a first-order chemical reaction with a rate constant k is assumed. Under these assumptions, the displacement can be modeled by the following equations

$$\phi\frac{\partial C}{\partial t} + u_x\frac{\partial C}{\partial x} + u_z\frac{\partial C}{\partial z} - \phi K_L\frac{\partial^2 C}{\partial x^2} - \phi K_T\frac{\partial^2 C}{\partial z^2} = \phi\kappa C \quad (1)$$

$$\frac{\partial u_x}{\partial x} + \frac{\partial u_z}{\partial z} = 0 \quad (2)$$

$$u_x = -\frac{k_x}{\mu_m}\left(\frac{\partial P}{\partial x} + \rho_m g \sin(\alpha)\right) \quad (3)$$

$$u_z = -\frac{k_z}{\mu_m}\left(\frac{\partial P}{\partial z} + \rho_m g \cos(\alpha)\right) \quad (4)$$

$$C = 0 \qquad \text{at } t = 0 \qquad \forall x, z \quad (5)$$

$$u_z = 0 \qquad \text{at } z = 0 \qquad \forall x,t \quad (6)$$

$$u_z = 0 \qquad \text{at } z = H \qquad \forall x, t \quad (7)$$

$$\frac{1}{H}\int_0^H u_x\, dz = u_T \qquad \text{at } x = 0 \qquad \forall t \quad (8)$$

$$P = P_{wf} + \bar{\rho} g \cos(\alpha)\,(H - z) \qquad \text{at } x = L \qquad \forall z, t \quad (9)$$

$$\bar{\rho} = \rho_o + \Delta\rho\frac{\int_0^H u_x\, dz}{Hu_o} \qquad \text{at } x = L \qquad \forall t \quad (10)$$

where $\Delta\rho = \rho_s - \rho_o$. The viscosity and density (μ_m and ρ_m) are functions of the concentration C of the invading fluid.

The procedure for inspectional analysis is shown in detail in the Appendix. It involves the introduction of two arbitrary scale factors for each of the variables in the equations. These scaling factors are linear transformations from the dimensional to dimensionless space. They are grouped into dimensionless scaling groups. Their values are then selected in such a way to minimize the number of groups. After this procedure is carried through, 10 dimensionless scaling groups were obtained (eqs A-13 to A-22).

These scaling groups are not linearly independent. To reduce the number of these scaling groups to linear independent scaling groups, the rank of the nonsquare "coefficient matrix" is determined. The minimum number of independent scaling groups is equal to the rank of the coefficient matrix. It was found that there are nine independent dimensionless scaling groups that describe miscible displacement of oil in a two-dimensional, homogeneous, anisotropic, porous medium with constant porosity and dip angle (eqs A-23 to A-31). These scaling groups are

$$P_{e_L} = (u_T/\phi L)/K_L = \text{longitudinal Peclet number} \quad (A\text{-}23)$$

$$N_d = (L/H)\sqrt{K_T/K_L} = \text{dispersion number} \quad (A\text{-}24)$$

$$N_{DA} = K_L/\kappa L^2 = \text{Damkholer number} \quad (A\text{-}25)$$

$$M = \mu_o/\mu_s = \text{viscosity ratio} \quad (A\text{-}26)$$

$$N_\alpha = \alpha = \text{dip angle group} \quad (A\text{-}27)$$

(29) Perkins, F. M.; Collins, R. E. Scaling Laws for Laboratory Flow Models of Oil Reservoirs. *Trans. AIME* **1960**, *219*, 383−385.

(30) Van Daalen, F.; Van Domselaar, H. R. Scaled Fluid-Flow Models with Geometry Differing from that of Prototype. *Soc. Pet. Eng. J.* **1972**, *12*, 220−228.

$$N_g = k_x \Delta\rho g/\mu_o u_T = \text{gravity number} \quad \text{(A-28)}$$

$$R_L = (L/H)\sqrt{k_z/k_x} = \text{effective aspect ratio} \quad \text{(A-29)}$$

$$N_\rho = \Delta\rho/\rho_o = \text{density number} \quad \text{(A-30)}$$

$$A_r = L/H = \text{aspect ratio} \quad \text{(A-31)}$$

If the molecular diffusion is negligible, the longitudinal Peclet number and the dispersion number become

$$P_{e_L} = L/\alpha_L$$

$$N_d = (L/H)\sqrt{\alpha_T/\alpha_L}$$

The dimensionless solvent concentration for miscible displacement can therefore be expressed in the following generalized form:

$$C_D = f(x_D, z_D, t_D, P_{e_L}, N_d, N_{DA}, M, N_\alpha, N_g, R_L, N_\rho, A_r) \quad (11)$$

Equation 11 applies to any geometrically similar porous medium. These scaling groups are not unique, but they represent the minimum number required to scale miscible displacements in a two-dimensional, homogeneous, anisotropic vertical cross section. The group N_d is original to this work.

Consider now a case of miscible displacement in a vertical cross-sectional porous medium under vertical equilibrium. In vertical equilibrium, the pressure gradient is independent of the *z*-direction. Under the assumption of vertical equilibrium and as shown by Shook et al.[25] for the case of immiscible displacement, the dimensionality of the governing equations, eqs 1−10, can be reduced. Application of the scaling procedure on the reduced equations yields the same groups except that the effective aspect ratio, R_L, is absent. This is because the recovery history, mixing zones, and saturation profiles are independent of R_L when vertical equilibrium (VE) is present.[2] Therefore, under VE, the dimensionless solvent concentration can be expressed as

$$C_D = f(x_D, z_D, t_D, P_{e_L}, N_d, N_{DA}, M, N_\alpha, N_g, N_\rho, A_r) \quad (12)$$

Effect of Groups on Oil Recovery

The effect of P_{e_L}, N_{DA}, M, N_α, R_L, and A_r on miscible displacements has been the subject of other studies in the literature.[31−34] Therefore, the sensitivity of only the gravity number (N_g), the dispersion number (N_d), and the density number (N_ρ) on the performance of miscible displacements is investigated here.

Effect of Gravity Number. One of the most important phenomena of a vertical cross-sectional displacement when a less dense fluid displaces a more dense fluid is gravity segregation. At low rates, gravity override will occur leading to early breakthrough of the injected fluid and poor oil recovery. However, at high flow rates, due to the unfavorable mobility ratio, viscous fingering will dominate the displacement resulting in bypassing of oil.

Chart 1. Schematic Layout of the Eight Simulated Miscible Displacements for Various Gravity Numbers

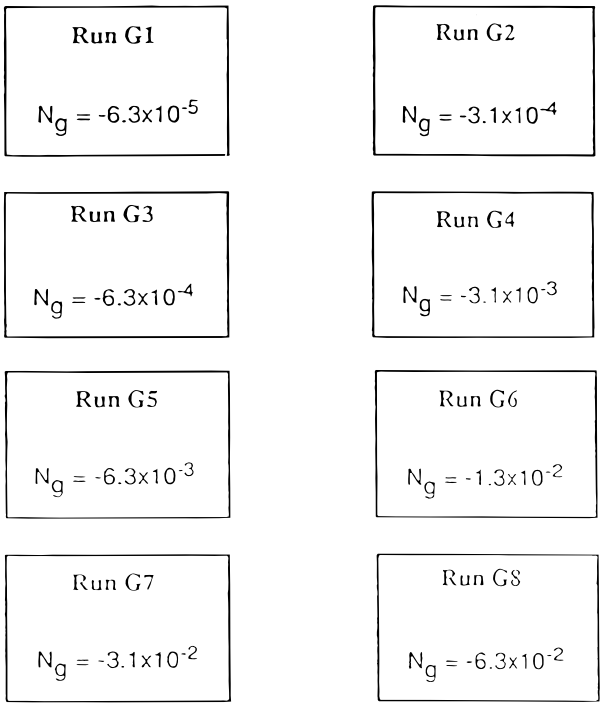

A number of vertical cross-sectional ($x-z$) simulation runs were made to investigate the effect of the gravity number on the behavior of unstable miscible displacements. A total of eight vertical cross-sectional simulation runs were made to cover a wide range of the gravity number, N_g. It should be noted that a higher N_g means higher gravity forces compared to the viscous forces. Other scaling groups were maintained constant in all the simulation runs. The eight simulation runs were carried out in geometrically similar porous media. Chart 1 shows a schematic layout of the eight simulation runs with their gravity numbers. The gravity number ranged from $N_g = -6.3 \times 10^{-5}$ for run G1 to $N_g = -6.3 \times 10^{-2}$ for run G8. All the figures in this section will be presented using a similar layout to Chart 1. By plotting all the results in the same figure, one can easily make at least a qualitative comparison of the displacement patterns. The quarter-power mixing rule was used in the simulator to estimate the mixture viscosity. We have used this rule in our earlier studies, and it gave acceptable predictions when compared to laboratory core flood experiments.[4] The quarter-power mixing rule is defined as

$$(1/\mu_m)^{1/4} = C_s(1/\mu_s)^{1/4} + C_o(1/\mu_o)^{1/4} \quad (13)$$

Figure 2 shows the simulated solvent concentration maps for the eight runs at 0.25 pore volumes injected.

(31) Crane, F. E.; Kendall, H. A.; Gardner, G. H. F. Some Experiments in the Flow of Miscible Fluids of Unequal Density Through Porous Media. *Soc. Pet. Eng. J.* **1963**, *December*, 277−280.

(32) Van Der Poel, C. Effect of Lateral Diffusivity on Miscible Displacement in Horizontal Reservoirs. *Trans. AIME* **1962**, *225*, 317−326.

(33) Kelkar, B. G.; Gupta, S. P. The effects of Small Heterogeneities on the Effective Dispersivity of Porous Medium. Paper SPE 17339, presented at the SPE/DOE Enhanced Oil Recovery Symposium, Tulsa, OK, 1988.

(34) Moissis, D. E., Miller, C. E.; Wheeler, M. F. A Parametric Study of Viscous Fingering in Miscible Displacement by Numerical Simulation. Proceedings for IMA Workshop on Numerical Simulation in Oil Recovery, MA, December, 1986.

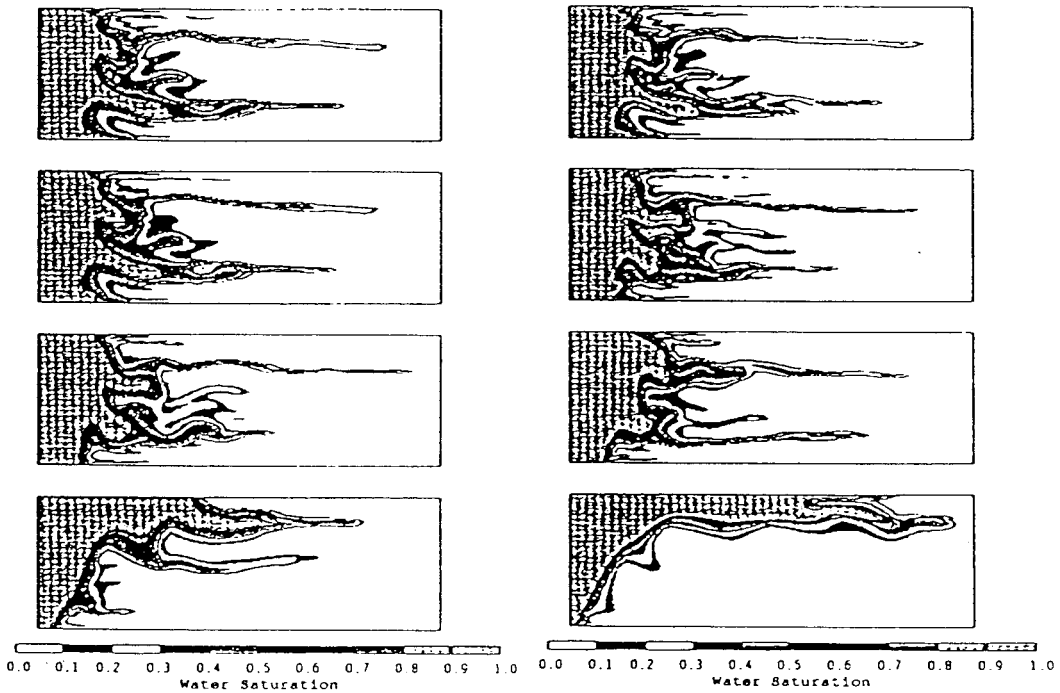

Figure 2. Effect of the gravity number on the simulated solvent concentration maps at 0.25 pore volume injected.

This method of presentation of the solvent concentration maps gives a clear picture of the transition from viscous-dominated to gravity-dominated displacement. At high rates (e.g. run G1 and run G2), the flow behavior is dominated by viscous fingering. In contrast, at low rates (e.g. run G8), the flow behavior is dominated by gravity override. For intermediate rates (e.g. run G6 and run G7), the displacement is governed by both viscous and gravity forces. Therefore, the transition to gravity override dominated displacement occurs when N_g is in the order of -1.3×10^{-2} to -3.1×10^{-2}. However, experimental results in glass beads[31,32] show that this transition actually occurs when N_g is on the order of -8.4×10^{-3}.

Effect of Dispersion Number. The effect of dispersion on unstable miscible displacements has been observed to be very significant by Kelkar and Gupta.[33] For this reason, a sensitivity study was conducted to examine the effect of the dispersion number on the behavior of unstable miscible displacements. Unlike other investigators,[33,34] no emphasis was placed on evaluating the effect of dispersion on the recovery curve. Rather, emphasis was placed on evaluating its effects on the solvent concentration distributions in the porous medium.

In order to test the sensitivity of the behavior of unstable miscible displacements to the dispersion number, four two-dimensional simulation runs (DP1, DP2, DP3, DP4) in a vertical cross section were performed. The dispersion numbers for the simulations are shown in Chart 2.

Figure 3 shows the solvent concentration maps for the four runs at 0.25 pore volumes injected. The figure shows that the effect of increasing the dispersion number is to reduce the degree of instability of the displacement. As the dispersion number increases, the number of active fingers decreases. Further increase in the dispersion number would result in no fingering. As a consequence, the displacement will become one-dimensional in nature for some limiting value of the dispersion number.

Chart 2. Schematic Layout of the Four Simulated Miscible Displacements for Various Dispersion Numbers

Run DP1 $N_d = 0$ $\alpha_T = 0.0$ cm	Run DP2 $N_d = 1.1$ $\alpha_T = 0.003$ cm
Run DP3 $N_d = 2.0$ $\alpha_T = 0.009$ cm	Run DP4 $N_d = 2.75$ $\alpha_T = 0.018$ cm

In addition, the variation of the dispersion number did not affect the mixing zone length. The mixing zone length is defined here as the average distance between the 0.10 and 0.90 concentration contours at 0.25 pore volume injected.

Effect of the Density Number. In order to investigate the effect of the density number on the behavior of miscible displacement, simulations were made at three density numbers ($N_\rho = 2$, 20, and 100) and two gravity numbers ($N_g = 6.3 \times 10^{-5}$ and 6.3×10^{-2}) for a total of six runs. They represent viscous-dominated displacements ($N_g = 6.3 \times 10^{-5}$) and gravity-dominated displacements ($N_g = 6.3 \times 10^{-2}$).

Figure 4 shows the solvent concentration images for the viscous-dominated displacements ($N_g = 6.3 \times 10^{-5}$) at density numbers of 2, 20, and 100. The images are for 0.25 pore volume injected. It can be observed that the fluid distributions are identical for the three density numbers. Figure 5 shows the concentration maps for the gravity-dominated displacements ($N_g = 6.3 \times 10^{-2}$) at the three density numbers. Again, the fluid distribu-

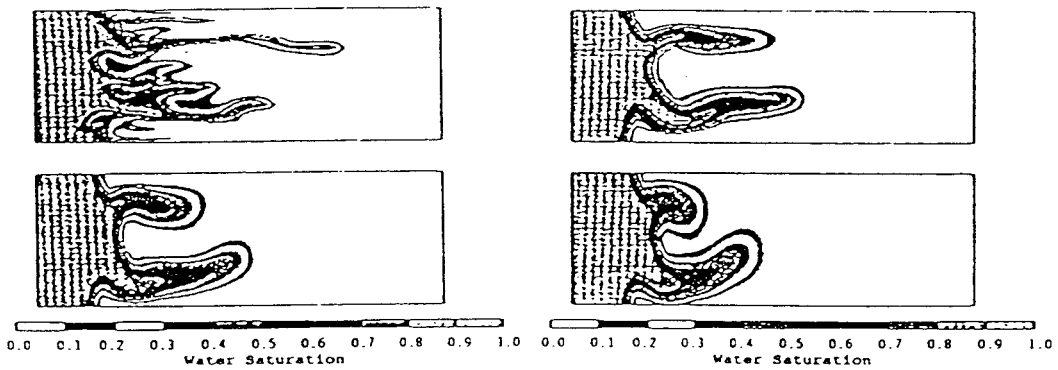

Figure 3. Effect of the dispersion number on the simulated solvent concentration maps at 0.25 pore volume injected.

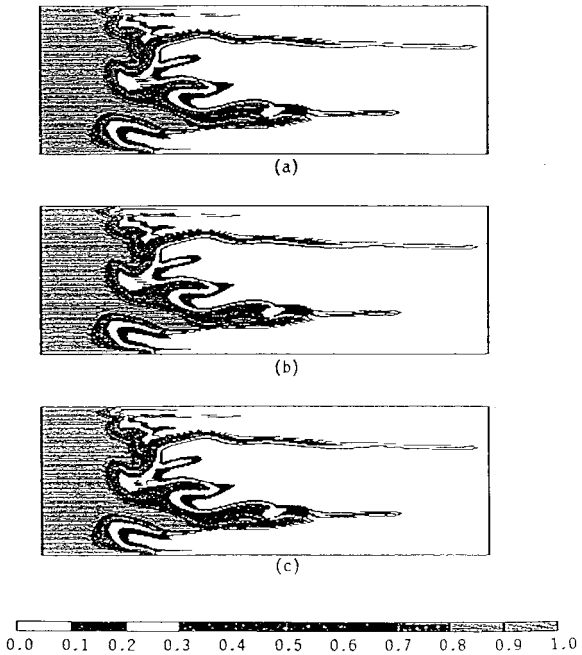

Figure 4. Simulated solvent concentration maps for $N_g = 6.3 \times 10^{-5}$ at 0.25 pore volume injected: (a) $N_\rho = 2.0$, (b) $N_\rho = 20.0$, (c) $N_\rho = 100.0$.

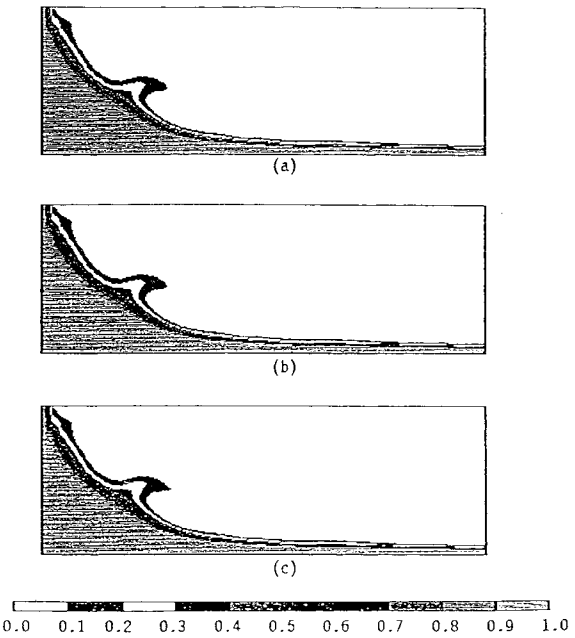

Figure 5. Simulated solvent concentrations maps for $N_g = 6.3 \times 10^{-2}$ at 0.25 pore volume injected: (a) $N_\rho = 2.0$, (b) $N_\rho = 20.0$, (c) $N_\rho = 100.0$.

tions are identical, and the oil recoveries are independent of the density number. More simulations were performed with a wider range of density number (from 0 to 100), and the same behavior was observed. Therefore, the density scaling group does not affect the miscible displacement. The dimensionless solvent concentration for unstable miscible displacement can therefore be expressed in the following generalized form:

$$C_D = f(x_D, z_D, t_D, P_{e_L}, N_d, N_{DA}, M, N_\alpha, N_g, R_L, A_r) \quad (14)$$

Evaluation of a Preliminary Neural Network Model

In order to check the ability of artificial neural networks to effectively model miscible displacements, a preliminary neural network model was prepared. The data used to train the network was obtained from simulation studies. At the present time of preliminary evaluation, only the effect of pore volume injected, dispersion number, and gravity number on the fractional oil recoveries are studied. The back-propagation with momentum and with an adaptive learning rate is used for training as described in detail in our earlier publications.[5−7]

Several neural network architectures were tried, and a one hidden layer network with 10 neurons was found to give acceptable predictions (Figure 6). The SSE for this network was 0.00065%, and the average percent error was 1.95%. Figures 7 and 8 give a comparison of the predictions of this neural network with those of the simulation results. Even though only few variations in the input patterns were considered, it can be concluded that an ANN is able to predict the fractional oil recovery for miscible displacement well. This is mainly due to the ability of neural networks to capture nonlinear functional patterns effectively.

Figure 7 also shows the variation of fractional oil recovery with the gravity number. The recovery remains essentially constant below a gravity number of 6.3×10^{-4} and decreases drastically above a value of -1.3×10^{-2}. For gravity numbers on the order of -6.3×10^{-4} to -1.3×10^{-2}, the oil recovery (on the average) increased by a small amount. This is where the transition from viscous-dominated to gravity-dominated displacement occurs. On the other hand, Figure 8 shows that the oil recovery tends to increase as the dispersion number or the pore volume injected increases.

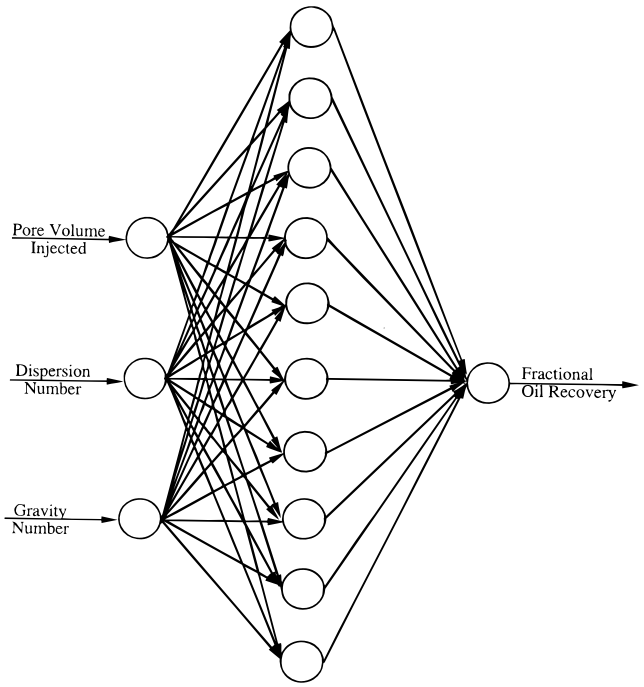

Figure 6. Architecture of the ANN used for predicting the fractional oil recovery.

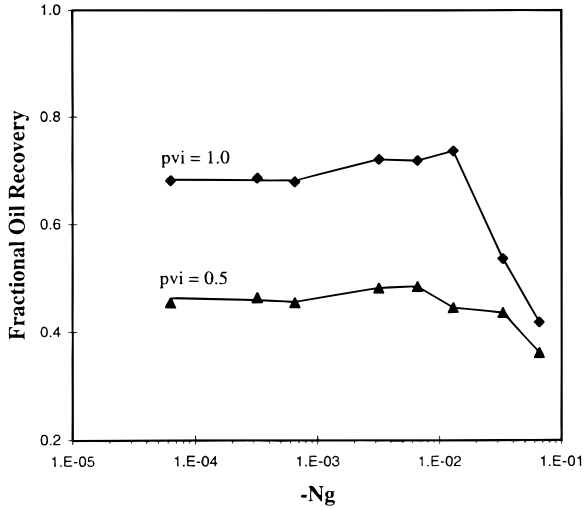

Figure 7. Comparison of the effect of the gravity number on the oil recovery, actual (pattern) and predicted (—) by the ANN.

Conclusion

A general procedure of inspectional analysis has been applied to derive the minimum number of dimensionless scaling groups which govern miscible displacements in a two-dimensional, homogeneous, anisotropic vertical cross section. Results show that in order to scale miscible displacements in porous media, it is required that nine dimensionless scaling groups be matched. However, through numerical sensitivity study, it was shown that one of the scaling groups did not have an effect on the performance of miscible displacements over all practical values. Thus, the number of dimensionless scaling groups has been reduced to eight. Three of the scaling groups were used as inputs to an ANN in order to predict the fractional oil recovery. Preliminary results indicate the suitability of ANN to offer good predictions.

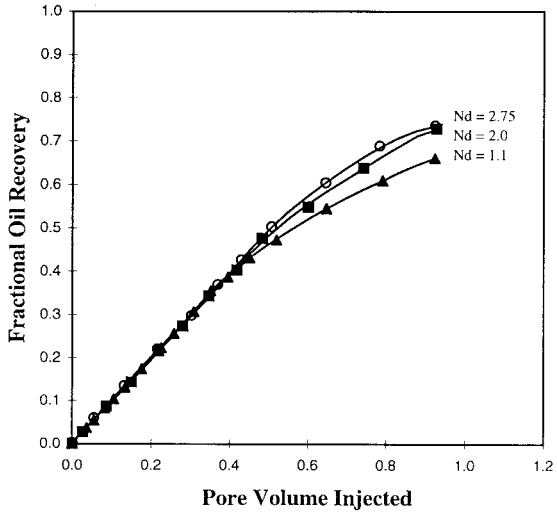

Figure 8. Comparison of the effect of the gravity number on the oil recovery, actual (pattern) and predicted (—) by the ANN.

Appendix

The displacement is modeled by the following conservation, continuity, and constitutive equations

$$\phi\frac{\partial C}{\partial t} + u_x\frac{\partial C}{\partial x} + u_z\frac{\partial C}{\partial z} - \phi K_L\frac{\partial^2 C}{\partial x^2} - \phi K_T\frac{\partial^2 C}{\partial z^2} = \phi\kappa C \quad \text{(A-1)}$$

$$\frac{\partial u_x}{\partial x} + \frac{\partial u_z}{\partial z} = 0 \quad \text{(A-2)}$$

$$u_x = -\frac{k_x}{\mu_m}\left(\frac{\partial P}{\partial x} + \rho_m g \sin(\alpha)\right) \quad \text{(A-3)}$$

$$u_z = -\frac{k_z}{\mu_m}\left(\frac{\partial P}{\partial z} + \rho_m g \cos(\alpha)\right) \quad \text{(A-4)}$$

$$C = 0 \quad \text{at } t = 0 \quad \forall x, z \quad \text{(A-5)}$$

$$u_z = 0 \quad \text{at } z = 0 \quad \forall x, t \quad \text{(A-6)}$$

$$u_z = 0 \quad \text{at } z = H \quad \forall x, t \quad \text{(A-7)}$$

$$\frac{1}{H}\int_0^H u_x\, dz = u_T \quad \text{at } x = 0 \quad \forall t \quad \text{(A-8)}$$

$$P = P_{wf} + \bar{\rho} g \cos(\alpha)\,(H - z) \quad \text{at } x = L \quad \forall z, t \quad \text{(A-9)}$$

$$\bar{\rho} = \rho_o + \Delta\rho\frac{\int_0^H u_x\, dz}{H u_o} \quad \text{at } x = L \quad \forall t \quad \text{(A-10)}$$

where $\Delta\rho = \rho_s - \rho_o$. The viscosity and density (μ_m and ρ_m) are functions of the concentration C of the invading fluid. To simplify the derivation of the scaling groups, a linear mixing rule is used to describe the mixture viscosity and density

$$\mu_m = \mu_o + C\Delta\mu \quad \text{(A-11)}$$

$$\rho_m = \rho_o + C\Delta\rho \quad \text{(A-12)}$$

where $\Delta\mu = \mu_s - \mu_o$. The results can be extended to other mixing rules (e.g. quarter-power mixing rule).

To nondimensionalize all these equations, let us define dimensionless variables such that

$$x = x_1^* x_D + x_2^*$$

$$z = z_1^* z_D + z_2^*$$

$$t = t_1^* t_D + t_2^*$$

$$u_x = u_{1x}^* u_{xD} + u_{2x}^*$$

$$u_z = u_{1z}^* u_{zD} + u_{2z}^*$$

$$P = P_1^* P_D + P_2^*$$

$$C = C_1^* C_D + C_2^*$$

In these transformations, the quantities with an asterisk (*) are constant quantities or scale factors, and the dimensionless variables are those with a subscript D. Substituting the transformations above into eqs A-1 to A-12, the following equations are obtained:

$$\phi\left(\frac{C_1^*}{t_1^*}\right)\frac{\partial C_D}{\partial t_D} + (u_{1x}^* u_{xD} + u_{2x}^*)\left(\frac{C_1^*}{x_1^*}\right)\frac{\partial C_D}{\partial x_D} + (u_{1z}^* u_{zD} + u_{2z}^*)\left(\frac{C_1^*}{z_1^*}\right)\frac{\partial C_D}{\partial z_D} - \phi K_L\left(\frac{C_1^*}{(x_1^*)^2}\right)\frac{\partial^2 C_D}{\partial x_D^2} - \phi K_T\left(\frac{C_1^*}{(z_1^*)^2}\right)\frac{\partial^2 C_D}{\partial z_D^2} = \phi\kappa(C_1^* C_D + C_2^*)$$

$$\left(\frac{u_{1x}^*}{x_1^*}\right)\frac{\partial u_{xD}}{\partial x_D} + \left(\frac{u_{1z}^*}{z_1^*}\right)\frac{\partial u_{zD}}{\partial z_D} = 0$$

$$(u_{1x}^* u_{xD} + u_{2x}^*) = -k_x[\mu_o + (C_1^* C_D + C_2^*)(\mu_s - \mu_o)]^{-1}\left(\left(\frac{P_1^*}{x_1^*}\right)\frac{\partial P_D}{\partial x_D} + (\rho_o + (C_1^* C_D + C_2^*)\Delta\rho)g\sin(\alpha)\right)$$

$$(u_{1z}^* u_{zD} + u_{2z}^*) = -k_z[\mu_o + (C_1^* C_D + C_2^*)(\mu_s - \mu_o)]^{-1}\left(\left(\frac{P_1^*}{z_1^*}\right)\frac{\partial P_D}{\partial z_D} + (\rho_o + (C_1^* C_D + C_2^*)\Delta\rho)g\cos(\alpha)\right)$$

$$(C_1^* C_D + C_2^*) = 0 \qquad \text{at } t_1^* t_D + t_2^* = 0 \qquad \forall\, x_D, z_D$$

$$(u_{1z}^* u_{zD} + u_{2z}^*) = 0 \qquad \text{at } z_1^* z_D + z_2^* = 0 \qquad \forall x_D, t_D$$

$$(u_{1z}^* u_{zD} + u_{2z}^*) = 0 \qquad \text{at } z_1^* z_D + z_2^* = H \qquad \forall x_D, t_D$$

$$\left(\frac{z_1^*}{H}\right)\int_0^{(H-z_2^*)/z_1^*} (u_{1x}^* u_{xD} + u_{2x}^*)\, dz_D = u_T \qquad \text{at } x_1^* x_D + x_2^* = 0 \qquad \forall t_D$$

$$(P_1^* P_D + P_2^*) = P_{wf} + \{\rho_o + \Delta\rho[(z_1^*/H)\int_0^{(H-z_2^*)/z_1^*} (u_{1x}^* u_{xD} + u_{2x}^*)\, dz_D/u_T]\} \times g\cos(\alpha)\,(H - z_1^* z_D - z_2^*) \qquad \text{at } x_1^* x_D + x_2^* = L \quad 0 \le z_1^* z_D + z_2^* \le H \qquad \forall t_D$$

Rearranging these equations to make them dimensionless yields the following equations:

$$\frac{\partial C_D}{\partial t_D} + \underset{\mathbf{1}}{\left(\frac{t_1^* u_{1x}^*}{\phi x_1^*}\right)} u_{xD}\frac{\partial C_D}{\partial x_D} + \underset{\mathbf{2}}{\left(\frac{u_{2x}^* t_1^*}{\phi x_1^*}\right)}\frac{\partial C_D}{\partial x_D} + \underset{\mathbf{3}}{\left(\frac{t_1^* u_{1z}^*}{\phi z_1^*}\right)} u_{zD}\frac{\partial C_D}{\partial z_D} + \underset{\mathbf{4}}{\left(\frac{u_{2z}^* t_1^*}{\phi z_1^*}\right)}\frac{\partial C_D}{\partial z_D} - \underset{\mathbf{5}}{\left(\frac{K_L t_1^*}{(x_1^*)^2}\right)}\frac{\partial^2 C_D}{\partial x_D^2} - \underset{\mathbf{6}}{\left(\frac{K_T t_1^*}{(z_1^*)^2}\right)}\frac{\partial^2 C_D}{\partial z_D^2} = \underset{\mathbf{7}}{(\kappa t_1^*) C_D} + \underset{\mathbf{8}}{\left(\frac{\kappa C_2^* t_1^*}{C_1^*}\right)}$$

$$\frac{\partial u_{xD}}{\partial x_D} + \underset{\mathbf{9}}{\left(\frac{u_{1z}^* x_1^*}{u_{1x}^* z_1^*}\right)}\frac{\partial u_{zD}}{\partial z_D} = 0$$

$$u_{xD} = -\left[\left[\underset{\mathbf{10}}{\left(\frac{C_1^* x_1^* u_{1x}^* \mu_o}{k_x P_1^*}\right)} - \underset{\mathbf{11}}{\left(\frac{C_1^* x_1^* u_{1x}^* \mu_s}{k_x P_1^*}\right)}\right] C_D + \underset{\mathbf{12}}{\left(\frac{C_2^* x_1^* u_{1x}^* \Delta\mu}{k_x P_1^*}\right)} + \underset{\mathbf{13}}{\left(\frac{x_1^* u_{1x}^* \mu_o}{k_x P_1^*}\right)}\right]^{-1}\left[\frac{\partial P_D}{\partial x_D} + \underset{\mathbf{14}}{\left(\frac{\Delta\rho g x_1^* C_1^*}{P_1^*}\right)} C_D \underset{\mathbf{15}}{\sin([\alpha])} + \underset{\mathbf{16}}{\left(\frac{\rho_o g x_1^*}{P_1^*}\right)}\sin(\alpha) + \underset{\mathbf{17}}{\left(\frac{\Delta\rho g x_1^* C_2^*}{P_1^*}\right)}\sin(\alpha)\right] - \underset{\mathbf{18}}{\left(\frac{u_{2x}^*}{u_{1x}^*}\right)}$$

$$u_{zD} = -\left[\left[\underset{\mathbf{19}}{\left(\frac{C_1^* z_1^* u_{1z}^* \mu_o}{k_z P_1^*}\right)} - \underset{\mathbf{20}}{\left(\frac{C_1^* z_1^* u_{1z}^* \mu_s}{k_z P_1^*}\right)}\right] C_D + \underset{\mathbf{21}}{\left(\frac{C_2^* z_1^* u_{1z}^* \Delta\mu}{k_z P_1^*}\right)} + \underset{\mathbf{22}}{\left(\frac{z_1^* u_{1z}^* \mu_o}{k_z P_1^*}\right)}\right]^{-1}$$

$$\left[\frac{\partial P_D}{\partial z_D} + \underset{\mathbf{23}}{\left(\frac{\Delta\rho g z_1^* C_1^*}{P_1^*}\right)}\cos(\alpha) C_D + \underset{\mathbf{24}}{\left(\frac{\rho_o g z_1^*}{P_1^*}\right)}\cos(\alpha) + \underset{\mathbf{25}}{\left(\frac{\Delta\rho g z_1^* C_2^*}{P_1^*}\right)}\cos(\alpha)\right] - \underset{\mathbf{26}}{\left(\frac{u_{2z}^*}{u_{1z}^*}\right)}$$

$$C_D = \underset{\mathbf{27}}{(-C_2^*/C_1^*)} \qquad \text{at } t_D = \underset{\mathbf{28}}{(-t_2^*/t_1^*)} \qquad \forall x_D, z_D$$

$$u_{zD} = (-u_{2z}^*/u_{1z}^*) \quad \text{(29)} \qquad \text{at } z_D = (-z_2^*/z_1^*) \quad \text{(30)} \qquad \forall x_D, t_D$$

$$u_{zD} = (-u_{2z}^*/u_{1z}^*) \quad \text{(31)} \qquad \text{at } z_D = ((H - z_2^*)/z_1^*) \quad \text{(32)} \qquad \forall x_D, t_D$$

$$\int_0^{((H-z_2^*)/z_1^*)} [u_{xD} + (u_{2x}^*/u_{1x}^*)] \, dz_D = (u_T H/z_1^* u_{1x}^*) \quad \text{(33)} \quad \text{(34)} \quad \text{(35)}$$

$$\text{at } x_D = (-x_2^*/x_1^*) \quad \text{(36)} \qquad \forall t_D$$

$$P_D = ((P_{wf} - P_2^*)/P_1^*) + [(\rho_o z_1^* g/P_1^*)\cos(\alpha) + (\Delta\rho z_1^* g/P_1^*)(z_1^* u_{1x}^*/H u_T)\cos(\alpha) \times \int_0^{((H-z_2^*)/z_1^*)} (u_{xD} + (u_{2x}^*/u_{1x}^*)) \, dz_D] (((H - z_2^*)/z_1^*) - z_D)$$

(37) (38) (39) (40) (41) (42) (43)

$$\text{at } x_D = ((L - x_2^*)/x_1^*), \quad \text{(44)}$$

$$(-z_2^*/z_1^*) \le z_D \le ((H - z_2^*)/z_1^*) \quad \text{(45)} \quad \text{(46)} \qquad \forall t_D$$

There are 46 dimensionless scaling groups in these equations which have been numbered for easy identification. The scale factors are arbitrary so they can be eliminated by setting the dimensionless groups equal to 0 or 1. However, the elimination process should not change the form of the original problem. In addition, nondimensionalizing should not eliminate the scale factors which multiply the dimensionless variables (x_D, z_D, t_D, etc.). Furthermore, the dimensionless time is chosen to begin at 0, while the dimensionless solvent concentration is chosen such that it varies between 0 and 1. Therefore, let us set groups: **8**, **12**, **18**, **21**, **26**, **27**, **28**, **30**, **36**, and **37** to 0 to obtain

$$t_2^* = u_{2x}^* = u_{2z}^* = x_2^* = z_2^* = 0$$

$$P_2^* = P_{wf} \qquad C_2^* = 0$$

Next, the groups **32** and **44** are set to 1 to obtain

$$z_1^* = H \qquad x_1^* = L$$

Now, if groups **1**, **3**, **10**, **13**, and **35** are also set to 1, then

$$u_1^* = u_T \qquad t_1^* = \phi L/u_T \qquad u_{1z}^* = u_T(H/L) \qquad P_1^* = \mu_o L u_T/k_x \qquad C_1^* = 1$$

Putting these scale factors back into all the equations yields the following dimensionless equations

$$\frac{\partial C_D}{\partial t_D} + u_{xD}\frac{\partial C_D}{\partial x_D} + u_{zD}\frac{\partial C_D}{\partial z_D} - \text{G1}\frac{\partial^2 C_D}{\partial x_D^2} - \text{G2}\frac{\partial^2 C_D}{\partial z_D^2} = \text{G3}\, C_D$$

$$(\partial u_{xD}/\partial x_D) + (\partial u_{zD}/\partial z_D) = 0$$

$$u_{xD} = -[(1 - \text{G4})C_D + 1]^{-1}((\partial P_D/\partial x_D) + \sin(\text{G5})\,(\text{G6}C_D + \text{G7}))$$

$$u_{zD} = -\text{G8}[(1 - \text{G4})C_D + 1]^{-1}((\partial P_D/\partial z_D) + \cos(\text{G5})(\text{G9}C_D + \text{G10}))$$

$$C_D = 0 \qquad \text{at } t_D = 0 \qquad \forall x_D, z_D$$

$$u_{zD} = 0 \qquad \text{at } z_D = 0 \qquad \forall x_D, t_D$$

$$u_{zD} = 0 \qquad \text{at } z_D = 1 \qquad \forall x_D, t_D$$

$$\int_0^1 u_{xD} \, dz_D = 1 \qquad \text{at } x_D = 0 \qquad \forall t_D$$

$$P_D = (\cos(\text{G5})(\text{G10} + \text{G9}\textstyle\int_0^1 u_{xD} \, dz_D))(1 - z_D) \qquad \text{at } x_D = 1, \quad 0 \le z_D \le 1 \qquad \forall t_D$$

where G1 to G10 are the remaining dimensionless scaling groups:

$$\text{G1} = \phi K_L/L u_T \tag{A-13}$$

$$\text{G2} = \phi K_T L/u_T H^2 \tag{A-14}$$

$$\text{G3} = \phi\kappa L/u_T \tag{A-15}$$

$$\text{G4} = \mu_s/\mu_o \tag{A-16}$$

$$\text{G5} = \alpha \tag{A-17}$$

$$\text{G6} = k_x\Delta\rho g/\mu_o u_T \tag{A-18}$$

$$\text{G7} = k_x\rho_o g/\mu_o u_T \tag{A-19}$$

$$\text{G8} = (k_z/k_x)(L^2/H^2) \tag{A-20}$$

$$\text{G9} = (k_x\Delta\rho g/\mu_o u_T)(H/L) \tag{A-21}$$

$$\text{G10} = (k_x\rho_o g/\mu_o u_T)(H/L) \tag{A-22}$$

Minimizing the Number of Scaling Groups. The same method used by Shook et al.[30] for immiscible displacement is used here to minimize the number of dimensionless scaling groups. In this method, the logarithm of both sides of eqs A-13 to A-22 is taken to render the equations linear. The resulting linear system of 10 equations with 15 unknowns is shown in Chart 3. Then, the rank of the resulting coefficient matrix is evaluated. The number of independent scaling groups is then equal to the rank of the coefficient matrix. The rank of the matrix is determined by the method of elementary row operations. Applying this method, the reduced coefficient matrix becomes

$$\begin{vmatrix} -1 & 0 & 0 & 0 & 0 & 0 & 0 & 0 & 0 & 0 & -1 & 1 & 1 & 0 & 0 \\ 2 & -2 & 0 & 0 & 0 & 0 & 0 & 0 & 0 & 0 & 0 & 0 & -1 & 1 & 0 \\ 2 & 0 & 0 & 0 & 0 & 0 & 0 & 0 & 0 & 0 & 0 & 0 & -1 & 0 & 1 \\ 0 & 0 & 0 & 0 & 1 & -1 & 0 & 0 & 0 & 0 & 0 & 0 & 0 & 0 & 0 \\ 0 & 0 & 0 & 0 & 0 & 0 & 0 & 0 & 0 & 1 & 0 & 0 & 0 & 0 & 0 \\ 0 & 0 & 0 & 1 & 0 & -1 & 1 & 0 & 1 & 0 & -1 & 0 & 0 & 0 & 0 \\ 0 & 0 & 0 & 0 & 0 & 0 & 1 & -1 & 0 & 0 & 0 & 0 & 0 & 0 & 0 \\ 2 & -2 & 1 & -1 & 0 & 0 & 0 & 0 & 0 & 0 & 0 & 0 & 0 & 0 & 0 \\ -1 & 1 & 0 & 0 & 0 & 0 & 0 & 0 & 0 & 0 & 0 & 0 & 0 & 0 & 0 \\ 0 & 0 & 0 & 0 & 0 & 0 & 0 & 0 & 0 & 0 & 0 & 0 & 0 & 0 & 0 \end{vmatrix}$$

Chart 3

$$\begin{vmatrix} \ln G1 \\ \ln G2 \\ \ln G3 \\ \ln G4 \\ \ln G5 \\ \ln G6 \\ \ln G7 \\ \ln G8 \\ \ln G9 \\ \ln G10 \end{vmatrix} = \begin{vmatrix} -1 & 0 & 0 & 0 & 0 & 0 & 0 & 0 & 0 & 0 & -1 & 1 & 1 & 0 & 0 \\ & -2 & 0 & 0 & 0 & 0 & 0 & 0 & 0 & 0 & -1 & 1 & 0 & 1 & 0 \\ 1 & 0 & 0 & 0 & 0 & 0 & 0 & 0 & 0 & 0 & -1 & 1 & 0 & 0 & 1 \\ 0 & 0 & 0 & 0 & 1 & -1 & 0 & 0 & 0 & 0 & 0 & 0 & 0 & 0 & 0 \\ 0 & 0 & 0 & 0 & 0 & 0 & 0 & 0 & 0 & 1 & 0 & 0 & 0 & 0 & 0 \\ 0 & 0 & 0 & 1 & 0 & -1 & 1 & 0 & 1 & 0 & -1 & 0 & 0 & 0 & 0 \\ 0 & 0 & 0 & 1 & 0 & -1 & 0 & 1 & 1 & 0 & -1 & 0 & 0 & 0 & 0 \\ 2 & -2 & 1 & -1 & 0 & 0 & 0 & 0 & 0 & 0 & 0 & 0 & 0 & 0 & 0 \\ -1 & 1 & 0 & 1 & 0 & -1 & 1 & 0 & 1 & 0 & -1 & 0 & 0 & 0 & 0 \\ -1 & 1 & 0 & 1 & 0 & -1 & 0 & 1 & 1 & 0 & -1 & 0 & 0 & 0 & 0 \end{vmatrix} \begin{vmatrix} \ln L \\ \ln H \\ \ln k_z \\ \ln k_x \\ \ln \mu_s \\ \ln \mu_o \\ \ln \Delta\rho \\ \ln \rho_o \\ \ln g \\ \alpha \\ \ln u_T \\ \ln \phi \\ \ln k_L \\ \ln k_T \\ \ln \kappa \end{vmatrix}$$

Hence, the rank of the matrix is equal to 9. After exponentiation, the remaining nine dimensionless scaling groups are

$$G1^* = \phi K_L/L u_T$$

$$G2^* = (L^2/H^2)(K_T/K_L)$$

$$G3^* = L^2\kappa/K_L$$

$$G4^* = \mu_s/\mu_o$$

$$G5^* = \alpha$$

$$G6^* = k_x\Delta\rho g/\mu_o u_T$$

$$G7^* = \Delta\rho/\rho_o$$

$$G8^* = (k_z/k_x)(L^2/H^2)$$

$$G9^* = H/L$$

Therefore, the final number of the independent scaling groups is nine (G1* to G9*). Considering the physical meaning of the scaling groups and the traditional terminology used, the following terms are now employed to define the scaling groups for miscible displacements:

$$P_{e_L} = 1/G1^* \qquad N_d = \sqrt{G2^*} \qquad N_{DA} = 1/G3^* \qquad M = 1/G4^*$$

$$N_\alpha = G5^* \qquad N_g = G6^* \qquad R_L = \sqrt{G7^*} \qquad N_\rho = G8^* \qquad A_r = 1/G9^*$$

Thus the scaling groups are now defined as

$$P_{e_L} = (u_T/\phi L)/K_L = \text{longitudinal Peclet number} \quad \text{(A-23)}$$

$$N_d = (L/H)\sqrt{K_T/K_L} = \text{dispersion number} \quad \text{(A-24)}$$

$$N_{DA} = K_L/\kappa L^2 = \text{Damkholer number} \quad \text{(A-25)}$$

$$M = \mu_o/\mu_s = \text{viscosity ratio} \quad \text{(A-26)}$$

$$N_\alpha = \alpha = \text{dip angle group} \quad \text{(A-27)}$$

$$N_g = k_x\Delta\rho g/\mu_o u_T = \text{gravity number} \quad \text{(A-28)}$$

$$R_L = (L/H)\sqrt{k_z/k_x} = \text{effective aspect ratio} \quad \text{(A-29)}$$

$$N_\rho = \Delta\rho/\rho_o = \text{density number} \quad \text{(A-30)}$$

$$A_r = L/H = \text{aspect ratio} \quad \text{(A-31)}$$

Nomenclature

C = solvent concentration
C_D = dimensionless solvent concentration
C_s, C_o = solvent and oil concentrations
g = gravitational acceleration
H = reservoir thickness
k_x, k_z = absolute permeability in the x- and in the z-directions
K_T = transverse dispersion coefficient
K_L = longitudinal dispersion coefficient
L = characteristic system length
M = viscosity ratio
N_{DA} = Damkholer number
N_g = gravity number
N_α = dip angle number
N_ρ = density number
P = pressure
P_{e_L} = longitudinal Peclet number
P_{V_i} = pore volume injected
P_{wf} = well flowing pressure
R_L = effective aspect ratio
t = time
t_D = dimensionless time
u_T = total flux (or superficial velocity)
u_x, u_z = flux in x- and z-directions
x, z = x- and z-directions
x_D, z_D = dimensionless x- and z-directions

Greek Symbols

ϕ = porosity
κ = chemical rate constant

α_L = longitudinal dispersivity
α_T = transverse dispersivity
ΔP = pressure drop across the porous medium
$\Delta\rho$ = density difference (solvent minus oil)
$\Delta\mu$ = viscosity difference (solvent minus oil)
α = dip angle (measured from horizontal counterclockwise)
μ_o, μ_s, μ_m = oil, solvent, and mixture viscosities
ρ_o, ρ_s, ρ_m = oil, solvent, and mixture densities

EF980020A